DCN
Version 1.0

August 2019
Version

Global Hyperspectral Imaging Spectral-library of Agricultural crops (GHISA)
Area of Study: Conterminous United States (CONUS)

Algorithm Theoretical Basis Document (ATBD)

USGS EROS
Sioux Falls, South Dakota

Document history

Document Version	Publication Date	Description
1.0	July 2019	Original
2.0	August 2019	1st revision

Contents

I. Members of the team

The Global Hyperspectral Imaging Spectral-library of Agricultural crops (GHISA) for the conterminous United States (CONUS) was produced by the following team members. Their specific role is mentioned below.

Dr. Prasad S. Thenkabail, Research Geographer, United States Geological Survey (USGS), is the Principal Investigator (PI) of the GHISA project. Dr. Thenkabail was instrumental in developing the conceptual framework of the project and the product. He made significant contribution in writing the manuscript, Algorithm Theoretical Basis Document (ATBD), User Guide, and providing scientific guidance on the GHISA project.

Dr. Itiya P. Aneece, Postdoctoral Research Geographer, USGS, with guidance from Dr. Thenkabail, preprocessed Hyperion images in Google Earth Engine, extracted spectra from the images, and compiled GHISA for the conterminous United States. She also contributed to the manuscript, ATBD, and User Guide.

II. Historical context, background, and need for GHISA

Agricultural crop characterization, modeling, mapping, and monitoring are crucial for accurately assessing crop traits, yields, and productivity (e.g., crop productivity, crop water productivity) which in turn helps in assessing and managing global food and water security. Since agricultural crops consume 80-90% of all human water use (Thenkabail et al., 2012, 2010), accurate cropland studies contribute to accurate water use assessments and crop water productivity assessments. Agricultural crop signatures greatly vary by crop type, growth stage, growing condition, management, soil type, climate, and a host of other factors (e.g., inputs like nitrogen, potassium, and phosphorous; pests, and diseases). Agricultural characteristics and traits can be well established using hyperspectral data that are acquired with clear and precise knowledge of various crop variables. Any such study requires us to gather hyperspectral libraries of crops taking into consideration all factors mentioned above. Vegetation or agricultural crop hyperspectral data are widely used in research as detailed in the new four-volume book-set on hyperspectral remote sensing of vegetation (Thenkabail et al. 2018 a, b, c, d) as well as numerous research papers (Oliphant et al. 2019, Teluguntla et al. 2018, Gumma et al. 2018, Aneece and Thenkabail 2018, Marshall et al. 2014, Mariotto et al. 2013, Thenkabail et al. 2013). These data are collected from various platforms (Ortenberg, 2018, Hoque and Phinn, 2018). Spaceborne sensors include the recently decommissioned United States of America's (USA) Earth Observing-1 (EO-1) Hyperion (Aneece et al. 2018, Moharana and Dutta 2016, Oskouei and Babakan 2016), Germany's Environmental Mapping and Analysis Program (EnMAP) (Bracken et al. 2019, Okujeni et al. 2015), the Italian Compact High Resolution Imaging Spectrometer (CHRIS) onboard of the Project for On Board Autonomy (PROBA) satellite (CHRIS PROBA) (Verrelst et al. 2012, Lin et al. 2019), the German Aerospace Center (German: Deutsches Zentrum für Luft- und Raumfahrt e.V.) or DLR's Earth Sensing Imaging Spectrometer (DESIS) (Krutz et al. 2019), and upcoming US NASA's SBG (formerly known as HyspIRI; Lee et al. 2015, Iqbal et al. 2018, Clark 2017), and the Japanese Hyperspectral Imager Suite (HISUI) (Matsunaga et al. 2018). Airborne sensors include NASA's Airborne Visible InfraRed Imaging Spectrometer- Next Generation (AVIRIS-NG) (Bhattacharya et al. 2019, Ratheesh et al. 2019, Chaube et al. 2019, Jha et al. 2019), the US Hyperspectral Digital Imagery Collection Experiment (HYDICE) (Zhang et al. 2006),

Hyperspectral Sensor Surveying (AISA-EAGLE) (Mansour et al. 2012, Lausch et al. 2015, Abdel-Rahman et al. 2015), hyperspectral imaging sensor (HyMap) (Riaza et al. 2014, Buzzi et al. 2014), Compact Airborne Spectrographic Imager (CASI) (Legleiter et al. 2016, Xu et al. 2018), AisaEAGLET (Doneus et al. 2014), and airborne Portable Remote Imaging SpectroMeter (PRISM) (Thompson et al. 2015, Mourolis et al. 2014). Drone-based sensors include Micro-Hyperspec X sensors (Dao et al. 2019, Guo et al. 2019), Rikola Hyperspectral camera (Ivushkin et al. 2019, Mozgeris et al. 2018), SOC710-GX (Rhee et al. 2018, Adao et al. 2017), Specim ImSpector V10 2/3 (Franceschini et al. 2017, Meij et al. 2017), OCI-UAV-1000 (Cahalane et al. 2017, Manfreda et al. 2018), and MicroHSI 410-SHARK (Manfreda et al. 2018). Ground-based sensors include ASD Field Spec (Salem 2017, Padghan and Deshmukh 2017), Ocean Optic USB4000 (Middleton 2010), and UniSpec DC Spectrometer Analysis System (Davidson et al. 2016). These data are collected and analyzed for various study sites in the world and the results are shared in reports and research papers. Unfortunately, the hyperspectral libraries of the crops or vegetation used in these papers are either not shared or shared by only a few researchers, often in an uncoordinated manner. Currently, **a systematic Global Hyperspectral Imaging Spectral-library of Agricultural crops (GHISA) does not exist**. The need for a GHISA is of utmost importance in the current scenario of increased availability of advanced hyperspectral sensors on various platforms (Ortenberg 2018, Hoque and Phinn 2018, Ghamisi et al. 2017, Panda et al. 2015). **GHISA is a** "*Comprehensive and systematic collection, collation, synthesis, standardization, and characterization of global agricultural crop hyperspectral signatures obtained from spaceborne, airborne (e.g., aircrafts, drones), platform-mounted, and ground-based hand-held spectroradiometers or imaging spectroscopy. The GHISA data are collected as near continuous spectra (e.g., every 1 or 10 nm) along a range of the electromagnetic spectrum (e.g., 400-2500 nm or 400-1000 nm or 8000-14000 nm). The collection and collation protocols of GHISA data are well defined and documented. GHISA data are processed using a standard set of protocols and algorithms for converting raw data into surface reflectance. Synthesis of GHISA data involves linking them to globally understood crop characteristics such as agroecological zones, precise geolocation, crop types, crop growing conditions, watering methods (e.g., irrigated or rainfed), and numerous other variables (e.g., inputs such as nitrogen applied, genome, etc). GHISA spectral libraries must have large sample sizes for each class to be robust. Characterization of GHISA data could include, for example, a comparison of hyperspectral narrowband data with multispectral broadband data for every crop type*" (Thenkabail and Aneece, this document). The need is multi-fold to understand, model, map, and monitor the following crop traits and/or help answer the following questions:

1. What are the typical hyperspectral signatures of individual agricultural crops? How do these hyperspectral signatures vary during different: (a) growth stages, (b) geographical area, (c) genomes, (d) management practices, (e) inputs, (f) and a host of other parameters (e.g., irrigation versus rainfed, soils)?
2. How does the same crop that is grown in different parts of the world change in its hyperspectral characteristics? Why?
3. How do hyperspectral signatures of crops acquired over an area for one season compare across years (e.g., during normal, drought, and wet years)?
4. What crop traits can be quantified by GHISA hyperspectral libraries? What are their accuracies?
5. How can technological advances over the years change the ability of the GHISA hyperspectral library to characterize a crop?
6. How do hyperspectral crop characteristics vary from crop to crop?

7. What advances can be made in understanding, modeling, mapping, and monitoring agricultural crops using hyperspectral narrowband data as opposed to multispectral broadband data?
8. What unique hyperspectral vegetation indices (HVIs) are developed that help advance our understanding of agricultural crop characteristics relative to multispectral broadband data derived vegetation indices (MBVIs)? What unique crop characteristics that cannot be characterized by MBVIs are characterized by HVIs?
9. How do the GHISA hyperspectral signatures of a particular crop acquired from different platforms (e.g., spaceborne, airborne, ground-based) compare and/or contrast?
10. How can GHISA help local, regional, federal, and international entities make informed decisions on agricultural practices?

In a nutshell, GHISA provides a knowledge-bank of agricultural crops of the world grown in different countries, regions, agroecological zones, and conditions. It will serve many purposes of scientific and practical applications. For example, GHISA will be a signature bank for training algorithms for crop type mapping or to establish their quantitative traits to develop crop biophysical and biochemical models (Aneece and Thenkabail, 2018).

III. Hyperspectral and reference input data

1. EO-1 Hyperion hyperspectral data

This Algorithm Theoretical Basis Document (ATBD) provides a detailed account of the GHISA product, which is generated using Earth Observing-1 (EO-1) spaceborne hyperspectral Hyperion satellite sensor data. There are 70,000+ EO-1 Hyperion hyperspectral images (Figure 1) acquired over 2000 to 2015 time-frame and available for free from USGS EarthExplorer (https://earthexplorer.usgs.gov/). For the full description of the EO-1 Hyperion data please refer to Barry (2001), Khurshid et al. (2006), and Scheffler and Karrasch (2014).

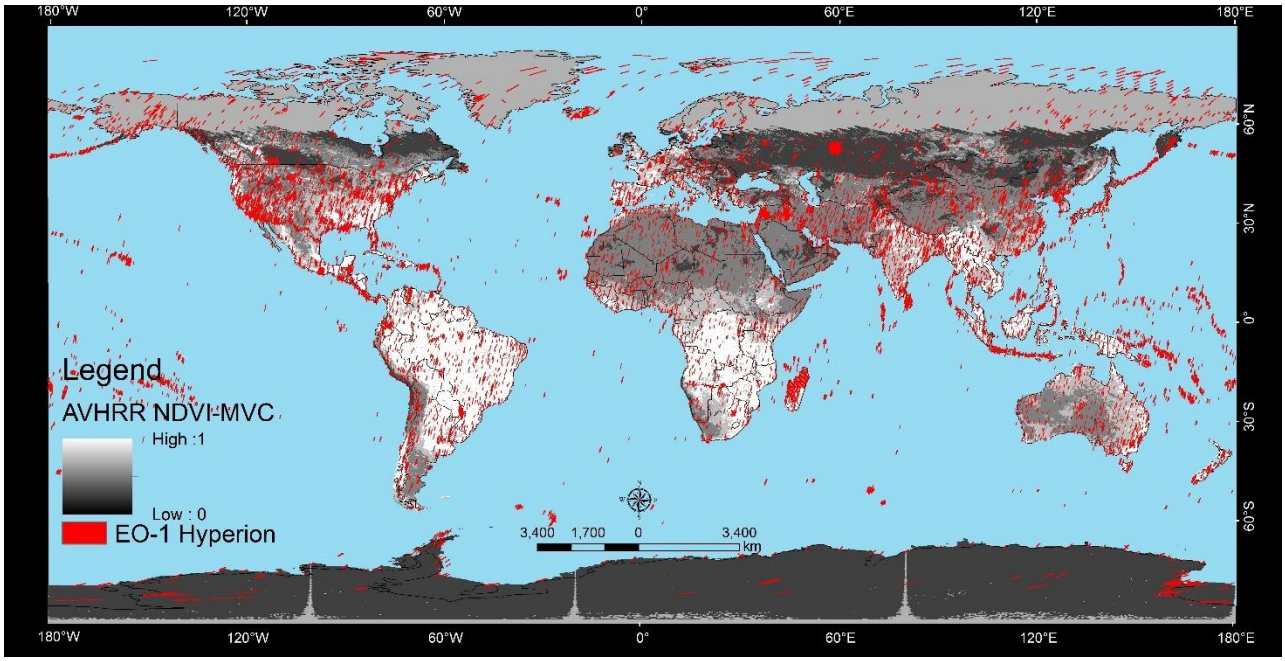

Figure 1. Spaceborne EO-1 Hyperion hyperspectral data acquired over the world from year 2000 to 2015. Over 70,000+ images are available for free download from the USGS EarthExplorer (https://earthexplorer.usgs.gov/). Each image is 185 km x 7.5 km and has 242 spectral bands each 10 nanometer wide in 400-2500 nm range (Source: Thenkabail et al., 2012).

This document describes the GHISA production scheme for the conterminous United States (CONUS) based on EO-1 Hyperion data acquired in various agroecological zones of USA over multiple sites (Table 1, Figure 2). Detailed descriptions of these data are provided in Aneece and Thenkabail (2018) and Aneece et al. (2018). There were 66 EO-1 Hyperion images (Table 1), the location of which are shown in Figure 2. These are representative images for each agroecological zone (FAO, 2018) with each site or benchmark area (Figure 2) having multiple images (Table 1). Each benchmark area was selected based on multiple Hyperion images available for the site as well as availability of two or more major world crops (e.g., wheat, rice, corn, soybeans, cotton). Further, these crops were also studied for their growth stages (emergence/ very early vegetation, early-mid vegetation, late vegetation, critical, senescence, and harvest).

The 99 EO-1 Hyperion images (Table 1) were selected for CONUS for the 2008 to 2015 time-period because during this time the United States Department of Agriculture (USDA) reference data (see section III.2) were available for the entire CONUS. Hyperion data were selected because Hyperion is the only known source of spaceborne hyperspectral data covering the entire world consistently over long time-periods. Such data will enable a comprehensive and systematic study of the world's agricultural crops over multiple years. It is imperative to monitor crops and assess global food security, especially with increasing global populations, urbanization, and changing dietary preferences. Knowledge of crop types and crop growth stages can help assess crop productivity. Remote sensing can be used to classify vegetation, and hyperspectral remote sensing specifically can enable the differentiation of crop types and crop growth stages.

Table 1: Hyperion images in seven agroecological zones (AEZs) and the leading world crops

within these images. We used a total of 99 Hyperion hyperspectral images spread across seven agroecological zones (AEZs) from 2008 to 2015 in the US. The dominant leading world crops in each of these images are also shown. [Source: Aneece and Thenkabail, 2018].

	Number of Hyperion Images*			
AEZ**	Crop Type-Discrimination	Crop Growth Stage-Discrimination	Years	Crops
2	0	4	2011-2012	Cotton
5	1	12	2013-2015	Cotton, Winter Wheat
6	3	12	2011-2014	Corn, Soybean
7	2	2	2012	Corn, Rice
8	0	12	2008-2014	Corn
9	2	12	2008-2015	Corn, Cotton, Soybean, Winter Wheat
10	3	12	2009-2015	Corn, Soybean
Total	11	66	2008-2015	Corn, Cotton, Rice, Soybean, Winter Wheat

*Original Hyperion images contain 242 bands, out of which 198 are calibrated and available in Google Earth Engine. After removing problematic bands most affected by atmospheric noise, we retained 131 bands from 356 nm to 2577 nm.

**AEZs (agroecological zones) based on Food and Agriculture Organization (FAO) (FAO, 2018).

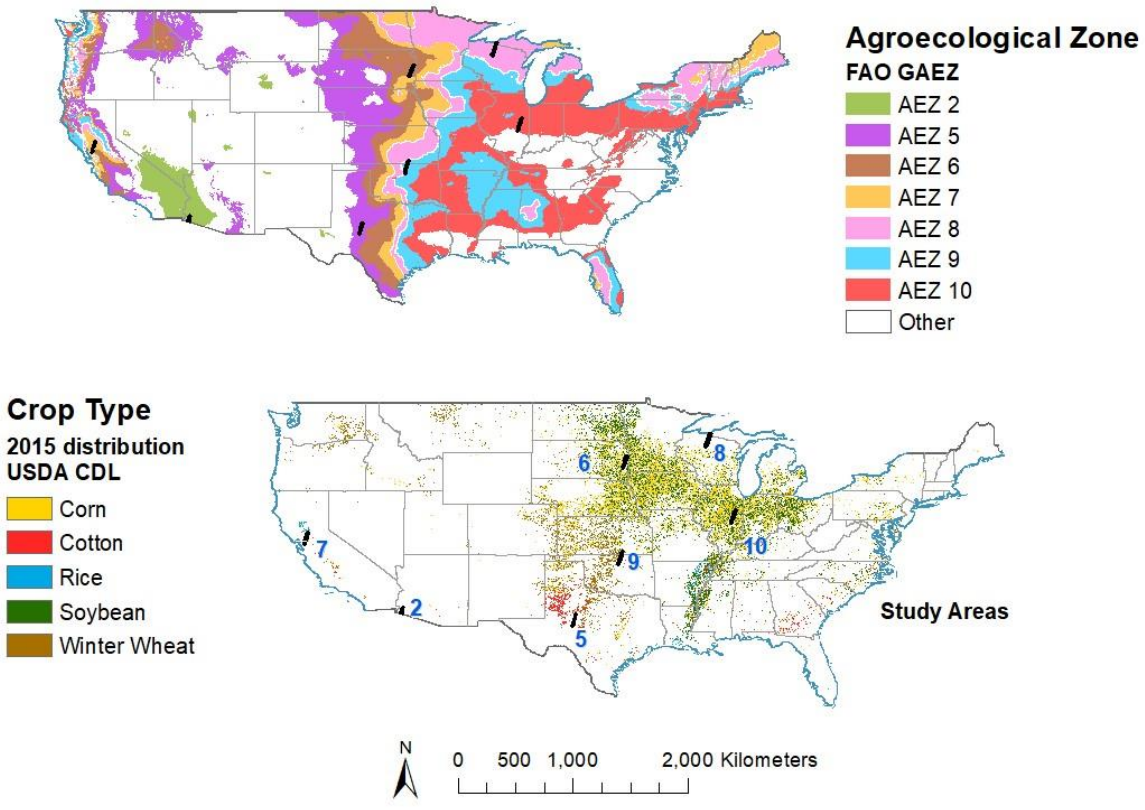

Figure 2. Study areas throughout the US in various agroecological zones. US study areas, named according to agroecological zones (AEZs) in which they are located. AEZs as defined by FAO (FAO, 2018). [Source: Aneece and Thenkabail, 2018].

2. Reference data

The USDA's Cropland Data Layer (CDL) (USDA, 2018a; https://nassgeodata.gmu.edu/CropScape/) was used as reference data to determine what crops exist in what precise location across the CONUS across the years corresponding to image acquisition dates (Table 1, Figure 2) and then extract hyperspectral libraries of crops for the GHISA spectral library. In addition to labeling spectra by crop type in GHISA, we have also labeled them by crop growth stages (emergence/very early vegetation, early-mid vegetation, late vegetation, critical, senescence, and harvest). These growth stages were estimated using the crop calendars generated by the Center for Sustainability and the Global Environment (SAGE) in University of Wisconsin-Madison (Sacks et al., 2010). These calendars were available for specific crop types in specific locations, across CONUS in different agroecological zones (Figure 2). They include planting and harvest dates, as well as monthly precipitation and temperature averages. We also inspected the spectral profiles to refine these labels.

IV. Algorithm description and data processing

Hyperion images were preprocessed in the JavaScript Application Programming Interface (API) of the Google Earth Engine (GEE) cloud-computing platform using the steps shown in Figure 3. To preprocess these images, we split the VNIR and SWIR data into separate images because they were collected by two different spectrometers and thus had different calibration requirements (Scheffler and Karrasch, 2014, Datt et al. 2003, Bannari et al. 2015, Pervez et al. 2016). We then converted VNIR and SWIR digital numbers to radiance by dividing digital numbers by 40 and 80 respectively (Barry 2001, Thenkabail et al. 2004, Thenkabail et al. 2013, Pervez et al. 2016). After recombining these datasets, we converted radiance to surface reflectance using the SMARTS radiative transfer model (Gueymard, 1995, 2001) (Figure 3). After cloud and cloud shadow masking, spectra were extracted from pixels corresponding with known crop type locations, using the USDA CDL as reference (USDA, 2018 a, b). These spectra were then smoothed using a 3-band moving average in R. The crop calendars designed by the Nelson Institute for Environmental Studies, SAGE, University of Wisconsin-Madison (Sacks et al., 2010) were used to estimate crop growth stages, refined by visual inspection of the spectra. Details on these steps, illustrated in Figure 3, are provided in 1a and 1b below. More details on preprocessing steps are also provided in Aneece et al. (2018).

The data processing to derive GHISA spectral library of agricultural crops for the entire CONUS area of USA is provided in section III and its subsections. The entire EO-1 Hyperion dataset of the CONUS area (Figure 1, and the subset used in this study: Figure 2, Table 1) is available in GEE for the entire US from 2008 to 2015. These raw images are ingested into GEE by the GEE team and are readily available to the user for preprocessing. Accurate reference data on crop types corresponding to these images are available through the USDA
CDL-(USDA,-2018b;
https://www.nass.usda.gov/Research_and_Science/Cropland/metadata/meta.php). Crop growth stage data were derived based on the SAGE dataset (SAGE, 2019; https://nelson.wisc.edu/sage/data-and-models/crop-calendar-dataset/index.php).

The recently decommissioned hyperspectral satellite-borne sensor Hyperion collected over 70,000 images throughout the world, all of which are freely available through the USGS EarthExplorer and GEE. These images can be used to build a spectral library of crops in different areas, years, and growth stages. Sixty-six Hyperion images within GEE in seven agroecological zones throughout the US from 2008 to 2015 were used to map five globally dominant crops (corn, cotton, rice, soybean, and winter wheat) and their growth stages (emergence/very early vegetation, early-mid vegetation, late vegetation, critical, senescence, and harvest).

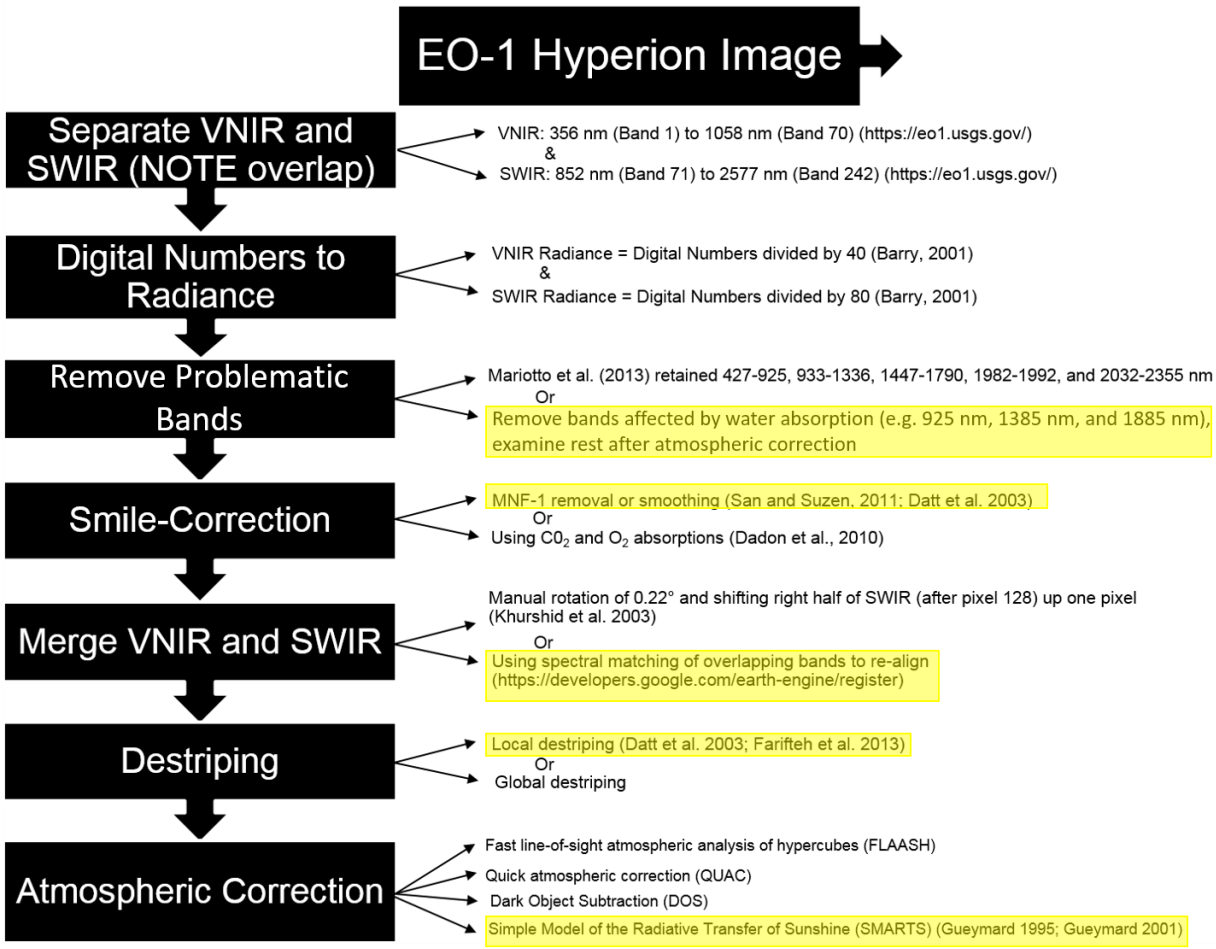

Figure 3. Example EO-1 Hyperion Pre-processing Workflow. These are the most common methods available for pre-processing steps; other methods exist. Highlighted methods are those the authors recommend. [Source: Aneece et al. 2018].

1. Algorithms

a. Algorithm details

Hyperion images were preprocessed in GEE. Cloud-computing allows for the processing of large collections of images without limitations of personal storage space or personal computing power (Navulur et al., 2013). Thus, it facilitates research at large temporal and spatial extents that would

otherwise not be possible. For example, Padarian et al. (2015) conducted an analysis involving 654,000 Landsat images in approximately 100 hours in GEE, which would have taken one million hours otherwise. Since Hyperion images are already ingested into GEE, they could be visualized and analyzed within the platform. Using the JavaScript API, we preprocessed the Hyperion images using the following steps. Code for these steps is available through LP DAAC.

Hyperion data were collected by two spectrometers, one for the VNIR bands 1-70 and one for the SWIR bands 71-242 (Scheffler and Karrasch, 2014). These spectrometers have different calibration requirements (Scheffler and Karrasch, 2014), so we separated them into two datasets for conversion from digital numbers (DN) to radiance (Rad). This was done by dividing VNIR DN by 40, and SWIR DN by 80, as described by Barry (2001).

Next, radiance was converted to surface reflectance (SR) using the Simple Model of the Atmospheric Radiative Transfer of Sunshine (SMARTS) radiative transfer model (Gueymard, 1995, 2001). This model was found to be 25 times faster than the 6S model, with only a 5% difference in satellite data processing results (Seidel et al. 2010). To convert radiance to surface reflectance, Equation 1 (from Chavez, 1996 assuming no haze) was used, where L is at-satellite radiance in W m^{-2} sr^{-1} mm^{-1}, E_{sun} is solar irradiance in W m^{-2} sr^{-1} mm^{-1}, θ_z and θ_v are zenith and viewing angles respectively in radians, T is transmittance (unitless), and E_{down} is diffuse downwelling radiance. Transmittance (T) is calculated using Equation 2 (from Gueymard, 2001), where $T_{R\lambda}$ is Rayleigh transmittance (unitless) dependent on wavelength λ, $T_{o\lambda}$ is ozone transmittance (unitless), $T_{n\lambda}$ is nitrogen dioxide transmittance (unitless), $T_{g\lambda}$ is uniformly mixed gas transmittance (unitless), $T_{w\lambda}$ is water vapor transmittance (unitless), and $T_{a\lambda}$ is aerosol transmittance (unitless). These components were calculated using methods described by Gueymard (1995, 2001). E_{down} was calculated using Equations 3 and 4 (from Gopinathan and Polokoana, 1986), where τ_D is the dimensionless transmission coefficient for direct solar radiation (Liu and Jordan, 1960). For more details on atmospheric correction, please refer to Aneece and Thenkabail (2018) and Aneece et al. (2018).

$$SR = \frac{\pi * L}{\cos\theta_V * (E_{sun} * \cos\theta_Z * T + E_{down})} \quad (1)$$

$$T = T_{R\lambda} * T_{o\lambda} * T_{n\lambda} * T_{g\lambda} * T_{w\lambda} * T_{a\lambda} \quad (2)$$

$$E_{down} = E_{sun} * \tau_D \quad (3)$$

$$\tau_D = 0.2710 - (0.2939 * T) \quad (4)$$

After conversion to surface reflectance, we masked out clouds and cloud shadows before extracting spectra. Clouds were detected using threshold reflectance values in the blue band and the sum of reflectance in the red, green, and blue bands since clouds have very high reflectance in the visible region. Cloud shadows were detected using threshold reflectance values in the sum of bands in the NIR and SWIR regions, in which regions cloud shadows have very low reflectance. Threshold values depend on the image and user preference as to how conservative they want the mask to be. This is a very rudimentary mask, which also masks out some water bodies; that was acceptable for

this application, which only needed spectral signatures from cropland. However, if a user wants to also study water bodies, a more detailed mask should be constructed.

After masking out clouds and cloud shadows, spectra were extracted from pixels with known crop types, using the USDA CDL as reference. These spectra were compiled into an Excel spreadsheet and problematic (noisy) bands were removed: 933-963 nm, 1114-1155 nm, 1336-1498 nm, 1780-2042 nm, and 2365-2396 nm. The spectra were then smoothed using a 3-band moving average. The R script for doing this is also available in LP DAAC.

The resulting spectra, along with image information, geographic coordinates, corresponding agroecological zone, crop type labels, and crop growth stage labels were compiled into the Global Hyperspectral Imaging Spectral-library of Agricultural crops (GHISA) for the US.

b. Programming and code

The Hyperion preprocessing steps were coded in GEE using the JavaScript Application Programming Interface (API). The code is available for download along with this ATBD.

3. Results

Using the 66 EO-1 Hyperion hyperspectral images of CONUS (Section III.1) and based on knowledge from the reference data (Section III.2), we derived the GHISA hyperspectral libraries of agricultural crops for their crop types (Figure 4, Table 2) and crop growth stages (Figure 5, Table 3).

Crop type reference training and validation data (Table 2) were gathered from 11 images across five AEZs for the five crops using USDA CDL data for reference. Illustrations of GHISA for example Hyperion images, with spectral averages by crop type are included in Figure 4. Overall, there were 2876 samples for training and 969 for validation. Across images, corn had 1104 training and 372 validation samples. Soybean had 1087 training and 366 validation samples. Winter wheat had 551 training and 184 validation samples. Rice had 86 training and 30 validation samples. Finally, cotton had 48 training and 17 validation samples. These data were used for crop type differentiation (Aneece and Thenkabail, 2018).

Crop growth stage reference training and validation data (Table 3) were gathered from 99 Hyperion images in seven AEZs for the five crops. An illustration of the Hyperion hyperspectral profiles averaged by crop growth stages is shown in Figure 5. Overall, there were 5184 samples for training and 1739 for validation. Corn had six growth stages represented, with a total of 1916 training and 641 validation samples. Soybean had all six growth stages represented, and 1563 training and 523 validation samples. Winter wheat had four growth stages represented with 6188 training and 2076 validation samples. Cotton had five growth stages represented, with 615 training and 208 validation samples. Lastly, Rice had two of the six growth stages represented, with 86 training and 30 validation samples. These data were used for crop growth stage differentiation (Aneece and Thenkabail, 2018).

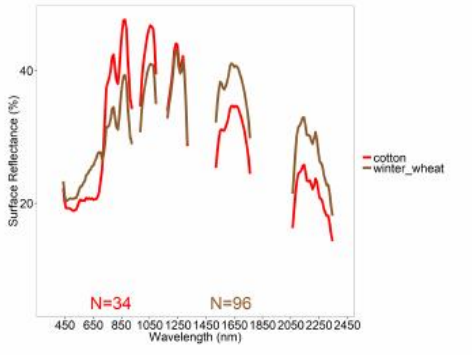

(a) GHISA for cotton and winter wheat in one Hyperion image from AEZ 5.

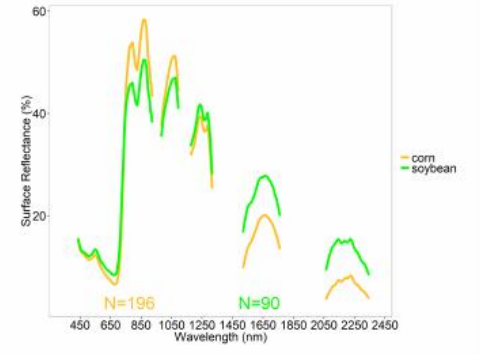

(b) GHISA for corn and soybean in one Hyperion image from AEZ 6.

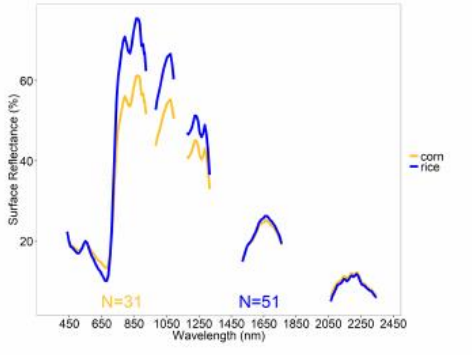

(c) GHISA for corn and rice in one Hyperion image from AEZ 7.

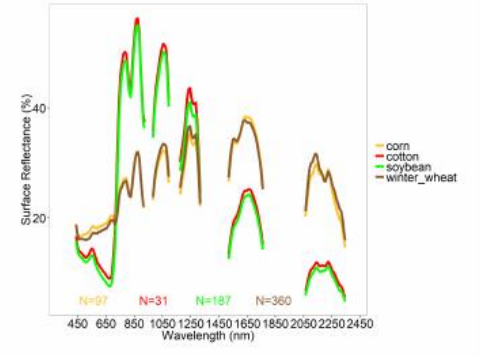

(d) GHISA for corn, cotton, soybean, and winter wheat in one Hyperion image from AEZ 9.

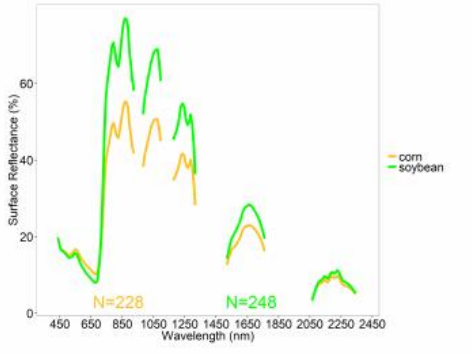

(e) GHISA for corn and soybean in one Hyperion image from AEZ 10.

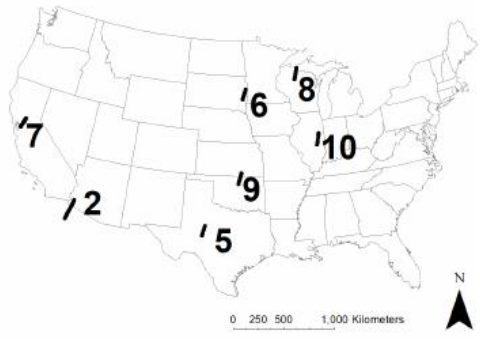

(f) US map showing locations of study areas.

Figure 4. Illustration of GHISA of the US for five crops. Global Hyperspectral Imaging Spectral library of Agricultural crops (GHISA) illustrated for five crops in particular agroecological zones and growth stages. N is number of spectra included in the average. [Source: Aneece and Thenkabail, 2018].

Table 2. Samples for crop type discrimination. Training and validation sample sizes for crop type discriminant analyses and image classification analyses; "other" only for image classification. [Source: Aneece and Thenkabail, 2018].

AEZ	Hyperion Image	Crop Type	Total Sample Size	Training Sample Size	Validation Sample Size
5	Image 1	Cotton	34	25	9
		Winter Wheat	96	72	24
		Other	260	195	65
6	Image 1	Corn	103	77	26
		Soybean	183	137	46
		Other	377	283	94
	Image 2	Corn	196	147	49
		Soybean	90	67	23
		Other	310	232	78
	Image 3	Corn	184	138	46
		Soybean	95	71	24
		Other	320	240	80
7	Image 1	Corn	34	25	9
		Rice	65	48	17
		Other	200	150	50
	Image 2	Corn	31	23	8
		Rice	51	38	13
		Other	200	150	50
9	Image 1	Corn	97	72	25
		Cotton	31	23	8
		Soybean	187	140	47
		Winter Wheat	360	270	90
		Other	1100	825	275
	Image 2	Corn	81	60	21
		Soybean	90	67	23
		Winter Wheat	279	209	70
		Other	936	702	234
10	Image 1	Corn	270	202	68
		Soybean	282	211	71
		Other	350	262	88
	Image 2	Corn	252	189	63
		Soybean	278	208	70
		Other	350	262	88
	Image 3	Corn	228	171	57
		Soybean	248	186	62
		Other	350	262	88

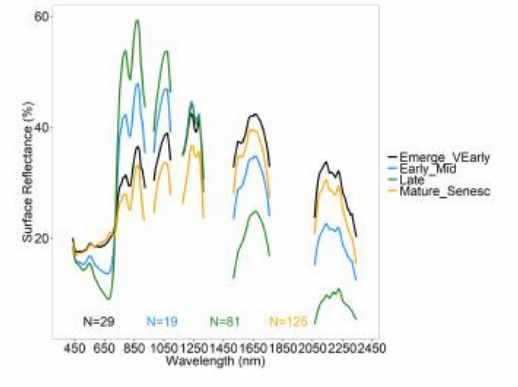

(a) GHISA of corn growth stages in AEZ 9.

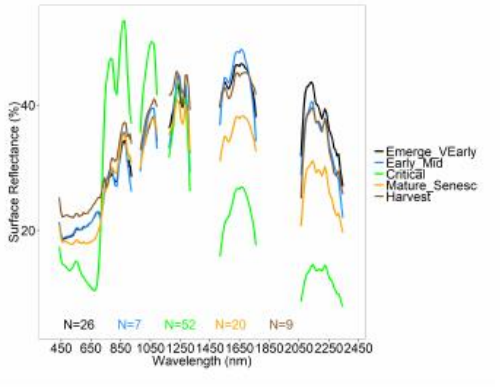

(b) GHISA of cotton growth stages in AEZ 9.

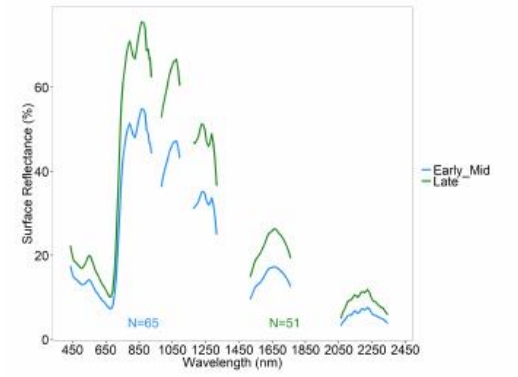

(c) GHISA of rice growth stages in AEZ 7.

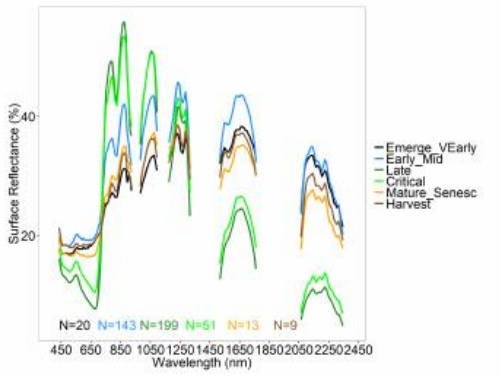

(d) GHISA of soybean growth stages in AEZ 9.

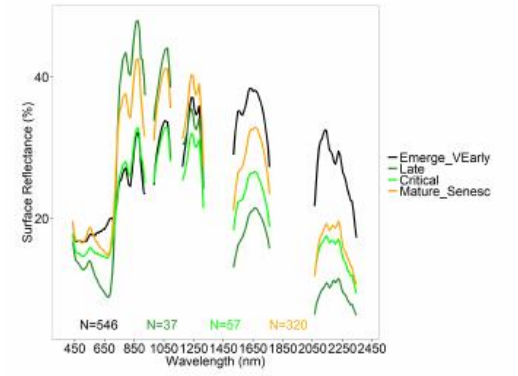

(e) GHISA of winter wheat growth stages in AEZ 9.

(f) US map showing locations of study areas.

Figure 5. Illustration of GHISA of the US for five crops. Global Hyperspectral Imaging Spectral library of Agricultural crops (GHISA) illustrated for one crop in two growth stages in AEZ 7, and four to six growth stages for the other crops in AEZ 9. N is number of spectra included in the average. [Source: Aneece and Thenkabail, 2018].

Table 3. Training and validation samples for crop growth stage discrimination. Training and validation sample sizes for discriminant analyses across crop types in seven agroecological zones (AEZs) using Global Hyperspectral Imaging Spectral library of Agricultural crops (GHISA) of the US for each crop in each of the six growth stages, where present, derived from Hyperion data. [Source: Aneece and Thenkabail, 2018].

Crop Type	AEZ	Number of Hyperion Images	Growth Stage	Sample Size (N) Total	Training	Validation
Corn	6, 8, 9, and 10	48	Emerge_VEarly	190	142	48
			Early_Mid	265	198	67
			Late	696	522	174
			Critical	779	584	195
			Mature_Senesc	499	374	125
			Harvest	128	96	32
Cotton	2, 5, and 9	25	Emerge_VEarly	215	161	54
			Early_Mid	316	237	79
			Critical	197	147	50
			Mature_Senesc	81	60	21
			Harvest	14	10	4
Rice	7	2	Early_Mid	65	48	17
			Late	51	38	13
Soybean	6, 9, and 10	36	Emerge_VEarly	132	99	33
			Early_Mid	581	435	146
			Late	291	218	73
			Critical	815	611	204
			Mature_Senesc	183	137	46
			Harvest	84	63	21
Winter Wheat	5 and 9	24	Emerge_VEarly	760	570	190
			Late	37	27	10
			Critical	70	52	18
			Mature_Senesc	474	355	119

V. Constraints and limitations

Constraints of the study included:

1. Limited availability of EO-1 Hyperion images during various growing periods;
2. Absence of wall-to-wall coverage of CONUS by EO-1 Hyperion limited more comprehensive development of GHISA, especially for crops not covered here;
3. Uncertainty in the reference CDL data. Although the CDL is the gold standard for crop type mapping in USA, uncertainties exist to an extent;
4. Signal to noise ratio of EO-1 Hyperion data

VI. Conclusions

This is the first ever attempt to develop a comprehensive Global Hyperspectral Imaging Spectral-library of Agricultural Crops (GHISA). We used 66 EO-1 Hyperion images for the 2008-2015 time-period along with USDA CDL reference data to develop GHISA hyperspectral libraries of agricultural crops of the conterminous United States (CONUS) on the basis of crops grown in various agroecological zones. GHISA of CONUS was developed for five major crops (corn, cotton, rice, soybean, and winter wheat). These hyperspectral libraries are made available for download through LP DAAC. Protocols for generating GHISA are available in this document and in Aneece and Thenkabail (2018) and Aneece et al. (2018). Code used in processing the EO-1 Hyperion data in GEE is downloadable in LP DAAC.

The goal of this effort is to build a comprehensive GHISA for the entire world using hyperspectral data from different platforms (e.g., spaceborne, airborne, drone-based, and ground-based) for the world's leading agricultural crops. In this specific effort, we developed GHISA for the conterminous United States (CONUS) based on EO-1 Hyperion data. We will continue this effort for other parts of the world and for CONUS using other platforms in the future. The GHISA releases come with user guides, ATBDs, and the data processing code whether performed in GEE or otherwise.

VII. Publications

Aneece, I.P. and Thenkabail, P.S. 2018. Accuracies achieved in classifying five leading world crop types and their growth stages using optimal Earth Observing-1 Hyperion hyperspectral narrowbands on Google Earth Engine. Remote Sensing Open Access Journal of MDPI. 10(12), 2027. Available at: https://pubs.er.usgs.gov/publication/70201462

Aneece, I., Thenkabail, P.S., Lyon, J., Huete, A. and Slonecker, T. 2018. Chapter 9 (of Volume I of Four-Volume Book): Spaceborne Hyperspectral EO-1 Hyperion Data Pre-Processing: Methods, Approaches, and Algorithms. Volume I Title: Fundamentals, Sensor Systems, Spectral Libraries, and Data Mining for Vegetation. Pp. 251-271. Book Title: "Hyperspectral Remote Sensing of Vegetation" (Second Edition, 4 Volume Set). Publisher: CRC Press- Taylor and Francis group, Boca Raton, London, New York. Pp. 450. (Editors: Thenkabail, P.S., Lyon, G.J., and Huete, A.). (Editors: Thenkabail, P.S., Lyon, G.J., and Huete, A.). IP-091722. Available at: https://www.routledge.com/Hyperspectral-Remote-Sensing-of-Vegetation-Second-Edition-FourVolume/Thenkabail-Lyon-Huete/p/book/9781138066250

VIII. Acknowledgements

This project was funded by the Mendenhall Postdoctoral Fellowship, United States Geological Survey (USGS). Support provided by the USGS Land Resources Mission Area (LRMA), and the National Land Imaging (NLI) and Land Change Science (LCS) programs are deeply appreciated.

IX. Contact information

LP DAAC User Services
U.S. Geological Survey (USGS)
Center for Earth Resources Observation and Science (EROS)
47914 252nd Street
Sioux Falls, SD 57198-0001
Phone Number: 605-594-6116
Toll Free: 866-573-3222 (866-LPE-DAAC)
Fax: 605-594-6963
Email: lpdaac@usgs.gov
Web: https://lpdaac.usgs.gov

For the Principal Investigators, feel free to write to:
Prasad S. Thenkabail at pthenkabail@usgs.gov
Itiya Aneece at ianeece@usgs.gov

X. Citations

Aneece, I. and Thenkabail, P. 2019. Global Hyperspectral Imaging Spectral-library of Agricultural crops (GHISA) for the Conterminous United States (CONUS). Algorithm Theoretical Basis Document (ATBD. NASA Land Processes Distributed Active Archive Center (LP DAAC). IP-110217.

XI. References

Abdel-Rahman, E., Makori, D., Landmann, T., Piiroinen, R., Gasim, S., Pellikka, P., and Raina, S. 2015. The Utility of AISA Eagle Hyperspectral Data and Random Forest Classifier for Flower Mapping. *Remote Sensing*, 7, 13298-13318.

Adao, T., Hruska, J., Padua, L., Bessa, J., Peres, E., Morais, R., and Sousa, J. 2017. Hyperspectral Imaging: A Review on UAV-Based Sensors, Data Processing and Applications for Agriculture and Forestry. *Remote Sensing*, 9, 1110.

Aneece, I.P. and Thenkabail, P.S. 2018. Accuracies achieved in classifying five leading world crop types and their growth stages using optimal Earth Observing-1 Hyperion hyperspectral narrowbands on Google Earth Engine. Remote Sensing Open Access Journal of MDPI. 10(12), 2027. Available at: https://pubs.er.usgs.gov/publication/70201462

Aneece, I., Thenkabail, P.S., Lyon, J., Huete, A. and Slonecker, T. 2018. Chapter 9 (of Volume I of Four-Volume Book): Spaceborne Hyperspectral EO-1 Hyperion Data Pre-Processing: Methods, Approaches, and Algorithms. Volume I Title: Fundamentals, Sensor Systems, Spectral Libraries, and Data Mining for Vegetation. Pp. 251-271. Book Title: "Hyperspectral Remote Sensing of Vegetation" (Second Edition, 4 Volume Set). Publisher: CRC Press- Taylor and Francis group, Boca Raton, London, New York. Pp. 450. (Editors: Thenkabail, P.S., Lyon, G.J., and Huete, A.). (Editors: Thenkabail, P.S., Lyon, G.J., and Huete, A.). IP-091722. Available at:

https://www.routledge.com/Hyperspectral-Remote-Sensing-of-Vegetation-Second-Edition-FourVolume/Thenkabail-Lyon-Huete/p/book/9781138066250

Bannari, A., Staenz, K., Champagne, C., and Khurshid, K. 2015. Spatial variability mapping of crop residue using Hyperion (EO-1) hyperspectral data. *Remote Sensing*, 7, 8107–8127.

Barry, P., 2001. EO-1/ Hyperion Science Data User's Guide, Level 1 b. Pub. Release, L1 B HYP.TO.01.077, TRW Space, Defense and Information Systems, Redondo Beach, CA.

Bhattacharya, B., Green, R., Rao, S., Saxena, M., Sharma, S., Kumar, K., Srinivasulu, P., Sharma, S., Dhar, D., Bandyopadhyay, S., Bhatwadekar, S., and Kumar, R. 2019. An overview of AVIRIS-NG airborne hyperspectral science campaign over India. *Current Science*, 116 (7), 1082-1088.

Bracken, A., Coburn, C., Staenz, K., Rochdi, N., Segl, K., Chabrillat, S., and Schmid, T. 2019. Detecting soil erosion in semi-arid Mediterranean environments using simulated EnMAP data. *Geoderma*, 340, 164-174.

Buzzi, J., Riaza, A., Garcia-Melendez, E., Weide, S., and Bachmann, M. 2014. Mapping Changes in a Recovering Mine Site with Hyperspectral Airborne HyMap Imagery (Sotiel, SW Spain). *Minerals*, 4, 313-329.

Cahalane, C., Walsh, D., Magee, A., Mannion, S., Lewis, P., and McCarthy, T. 2017. Sensor Pods: Multi-Resolution Surveys from a Light Aircraft. *Inventions*, 2, 2, doi:10.3390/inventions2010002

Chaube, N., Lele, N., Misra, A., Murthy, T., Manna, S., Hazra, S., Panda, M., and Samal, R. 2019. Mangrove species discrimination and health assessment using AVIRIS-NG hyperspectral data. *Current Science*, 116 (7), 1136-1142.

Chavez, P., Jr. 1996. Image-based atmospheric corrections- revisited and improved. *Photogrammetric Engineering & Remote Sensing*, 62, 1025–1036.

Clark, M. 2017. Comparison of simulated hyperspectral HyspIRI and multispectral Landsat 8 and Sentinel-2 imagery for multi-seasonal, regional land-cover mapping. *Remote Sensing of Environment*, 200, 311-325.

Dao, P., He, Y., and Lu, B. 2019. Maximizing the quantitative utility of airborne hyperspectral imagery for studying plant physiology: An optimal sensor exposure setting procedure and empirical line method for atmospheric correction. *International Journal of Applied Earth Observation and Geoinformation*, 77, 140-150.

Datt, B., McVicar, T., Van Niel, T,; Jupp, D., and Pearlman, J. 2003. Preprocessing EO-1 Hyperion hyperspectral data to support the application of agricultural indexes. *IEEE Transactions on Geoscience and Remote Sensing*, 41, 1246–1259.

Davidson, S., Santos, M., Sloan, V., Watts, J., Phoenix, G., Oechel, W., and Zona, D. 2016. Mapping Arctic tundra vegetation communities using field spectroscopy and multispectral

satellite data in North Alaska, USA. *Remote Sensing*, 8, 978.

Doneus, M., Verhoeven, G., Atzberger, C., Wess, M., and Rus, M. 2014. New ways to extract archaeological information from hyperspectral pixels. *Journal of Archaeological Science*, 52, 84-96.

eoPortal. 2019. ISS Utilization: HISUI (Hyperspectral Imager Suite). Available at: https://eoportal.org/web/eoportal/satellite-missions/content/-/article/iss-utilization-hisui-hyperspectral-imager-suite-

FAO—Food and Agriculture Organization of the United Nations. GAEZ-–Global Agro-Ecological Zones; FAO: Rome, Italy, 2018. Available at: http://www.fao.org/nr/gaez/en/

Franceschini, M., Bartholomeus, H., van Apeldoorn, D., Suomalainen, J., and Kooistra, L. 2017. Intercomparison of unmanned aerial vehicle and ground-based narrow band spectrometers applied to crop trait monitoring in organic potato production. *Sensors*, 17, 1428.

Ghamisi, P., Yokoya, N., Li, J., Liao, W., Liu, S., Plaza, J., Rasti, B., and Plaza, A. 2017. Advances in hyperspectral image and signal processing: A comprehensive overview of the state of the art. *IEEE Geoscience and Remote Sensing Magazine*, DOI: 10.1109/MGRS.2017.2762087.

Gopinathan, K., and Polokoana, P. 1986. Estimation of hourly beam and diffuse solar radiation. *Solar & Wind Technology*, 3, 223–229.

Gueymard, C., 1995. SMARTS2, a simple model of the atmospheric radiative transfer of sunshine: Algorithms and performance assessment. Technical Report FSEC-PF-270-95, Florida Solar Energy Center; University of Central Florida, Cocoa, FL.

Gueymard, C., 2001. Parameterized transmittance model for direct beam and circumsolar spectral irradiance. *Solar Energy*, 71(5), 325–346.

Gumma, M., Thenkabail, P.S., Deevi, K., Mohammed, I., Teluguntla, P., Oliphant, A., Xiong, J., Aye, T., and Whitbread, A. 2018. Mapping cropland fallow areas in Myanmar to scale up sustainable intensification of pulse crops in the farming system. *GIScience & Remote Sensing*, 55 (6), 926-949.

Guo, L., Zhang, H., Shi, T., Chen, Y., Jiang, Q., and Linderman, M. 2019. Prediction of soil organic carbon stock by laboratory spectral data and airborne hyperspectral images. *Geoderma*, 337, 32-41.

Hoque, M. and Phinn, S. 2018. Chapter 12: Methods for linking drone and field hyperspectral data to satellite data. Volume I Title: Fundamentals, Sensor Systems, Spectral Libraries, and Data Mining for Vegetation. Pp. 321-354. Book Title: "Hyperspectral Remote Sensing of Vegetation" (Second Edition, 4 Volume Set). Publisher: CRC Press- Taylor and Francis group, Boca Raton, London, New York. Pp. 450. (Editors: Thenkabail, P.S., Lyon, G.J., and Huete, A.). (Editors: Thenkabail, P.S., Lyon, G.J., and Huete, A.). IP-091722. Available at: https://www.routledge.com/Hyperspectral-Remote-Sensing-of-Vegetation-Second-Edition-

FourVolume/Thenkabail-Lyon-Huete/p/book/9781138066250

Iqbal, A., Ullah, S., Khalid, N., Ahmad, W., Ahmad, I., Shafique, M., Hulley, G., Roberts, D., and Skidmore, A. 2018. Selection of HyspIRI optimal band positions for the earth compositional mapping using HyTES data. *Remote Sensing of Environment*, 206, 350-362.

Ivushkin, K., Bartholomeus, H., Bregt, A., Pulatov, A., Franceschini, M., Kramer, H., van Loo, E., Roman, V., and Finkers, R. 2019. UAV based soil salinity assessment of cropland. *Geoderma*, 338, 502-512.

Jha, C., Rakesh, Singhal, J., Reddy, C., Rajashekar, G., Maity, S., Patnaik, C., Das, A., Misra, A., Singh, C., Mohapatra, J., Krishnayya, N., Kiran, S., Townsend, P., and Martinez, M. 2019. Characterization of species diversity and forest health using AVIRIS-NG hyperspectral remote sensing data. *Current Science*, 116 (7), 1124-1135.

Khurshid, K., Staenz, K., Sun, L., Neville, R., White, H., Bannari, A., Champagne, C., and Hitchcock, R. 2006. Preprocessing of EO-1 Hyperion data. *Canadian Journal of Remote Sensing*, 32 (2), 84-97.

Krutz, D., Muller, R., Knodt, U., Gunther, B., Walter, I., Sebastian, I., Sauberlich, T., Reulke, R., Carmona, E., Eckardt, A., Venus, H., Fischer, C., Zender, B., Arloth, S., Lieder, M., Neidhardt, M., Grote, U., Schrandt, F., Gelmi, S., and Wojtkowiak, A. 2019. The instrument design of the DLR Earth Sensing Imaging Spectrometer (DESIS). *Sensors*, 19, 1622.

Lausch, A., Salbach, C., Schmidt, A., Doktor, D., Merbach, I., and Pause, M. 2015. Deriving phenology of barley with imaging hyperspectral remote sensing. *Ecological Modelling*, 295, 123-135.

Lee, C., Cable, M., Hook, S., Green, R., Ustin, S., Mandl, D., and Middleton, E. 2015. An introduction to the NASA Hyperspectral InfraRed Imager (HyspIRI) mission and preparatory activities. *Remote Sensing of Environment*, 167, 6-19.

Legleiter, C., Overstreet, B., Glennie, C., Pan, Z., Fernandez-Diaz, J. and Singhania, A. 2016. Evaluating the capabilities of the CASI hyperspectral imaging system and Aquarius bathymetric LiDAR for measuring channel morphology in two distinct river environments. *Earth Surface Processes and Landforms*, 41, 344-363.

Lin, J., Pan, Y., Lyu, H., Zhu, X., Li, X., Dong, B., and Li, H. 2019. Developing a two-step algorithm to estimate the leaf area index of forests with complex structures based on CHRIS/PROBA data. *Forest Ecology and Management*, 441, 57-70.

Liu, B., and Jordan, R. 1960. The interrelationship and characteristic distribution of direct, diffuse, and total solar radiation. 1-19.

Manfreda, S., McCabe, M., Miller, P., Lucas, R., Madrigal, V., Mallinis, G., Dor, E., Helman, D., Estes, L., Ciraolo, G., Mullerova, J., Tauro, F., de lima, M., de Lima, J., Maltese, A., Frances, F., Caylor, K., Kohv, M., Perks, M., Ruiz-Perez, G., Su, Z., Vico, G., and Toth, B. 2018. On the Use of Unmanned Aerial Systems for Environmental Monitoring. *Remote Sensing*, 10, 641.

Mansour, K., Mutanga, O., Everson, T., and Adam, E. 2012. Discriminating indicator grass species for rangeland degradation assessment using hyperspectral data resampled to AISA Eagle resolution. *ISPRS Journal of Photogrammetry and Remote Sensing*, 70, 56-65.

Mariotto, I., Thenkabail, P., Huete, A., Slonecker, T., and Platonov, A. 2013. Hyperspectral versus multispectral crop-productivity modeling and type discrimination for the HyspIRI mission. *Remote Sensing of Environment*, 139, 291–305.

Marshall, M., and Thenkabail, P. 2014. Biomass modeling of four leading world crops using hyperspectral narrowbands in support of HyspIRI mission. *Photogrammetric Engineering & Remote Sensing*, 80, 757–772.

Matsunaga T., Iwasaki, A., Tsuchida, S., Iwao, K., Tanii, J., Kashimura, O., Nakamura, R., Yamamoto, H., Kato, S., Obata, K., Mouri, K., Yamamoto, S., Tachikawa, T. 2018. Hisui Status Toward FY2019 Launch, IGARSS 2018 - 2018 IEEE International Geoscience and Remote Sensing Symposium, Valencia, pp. 160-163. doi: 10.1109/IGARSS.2018.8518639

Meij, B., Koositra, L., Suomalainen, J., Barel, J., Deyn, G. 2017. Remote sensing of plant trait responses to field-based plant–soil feedback using UAV-based optical sensors. *Biogeosciences*, 14, 733-749.

Middleton, E. 2010. Diurnal and Directional Responses of Chlorophyll Fluorescence and the PRl in a Cornfield. 4th International Workshop on Remote Sensing of Vegetation Fluorescence, Valencia, Spain. Nov 15-17.

Moharana, S. and Dutta, S. 2016. Spatial variability of chlorophyll and nitrogen content of rice from hyperspectral imagery. *ISPRS Journal of Photogrammetry and Remote Sensing*, 122, 17–29.

Mourolis, P., Gorp, B., Green, R., Dierssen, H., Wilson, D., Eastwood, M., Boardman, J., Gao, B., Cohen, D., Franklin, B., Loya, F., Lundeen, S., Mazer, A., McCubbin, I., Randall, D., Richardson, B., Rodriguez, J., Sarture, C., Urquiza, E., Vargas, R., White, V., and Yee, K. 2014. Portable Remote Imaging Spectrometer coastal ocean sensor: design, characteristics, and first flight results. *Applied Optics*, 53 (7), 1363-1380.

Mozgeris, G., Juodkiene, V., Jonikavicius, D., Straigyte, L, Gadal, S., and Ouerghemmi, W. 2018. Ultra-light aircraft-based hyperspectral and colour-infrared imaging to identify deciduous tree species in an urban environment. *Remote Sensing*, 10, 1668.

Navulur, K., Lester, D., Marchetti, A., Hammann, G., 2013. Demystifying cloud computing for remote sensing applications. *Earth Imaging Journal*, pp.14–19.

Okujeni, A., Linden, S., and Hostert, P. 2015. Extending the vegetation–impervious–soil model using simulated EnMAP data and machine learning. *Remote Sensing of Environment*, 158, 69-80.

Oliphant, A. J., Thenkabail, P. S., Teluguntla, P., Xiong, J., Gumma, M. K., Congalton, R. G., & Yadav, K. 2019. Mapping cropland extent of Southeast and Northeast Asia using multi-year time-

series Landsat 30-m data using a random forest classifier on the Google Earth Engine Cloud. *International Journal of Applied Earth Observation and Geoinformation*, 81, 110-124.

Ortenberg, F. 2018. Chapter 2: Hyperspectral sensor characteristics: Airborne, spaceborne, hand-held, and truck-mounted; Integration of hyperspectral data with LiDAR. Volume I Title: Fundamentals, Sensor Systems, Spectral Libraries, and Data Mining for Vegetation. Pp. 41-69. Book Title: "Hyperspectral Remote Sensing of Vegetation" (Second Edition, 4 Volume Set). Publisher: CRC Press- Taylor and Francis group, Boca Raton, London, New York. Pp. 450. (Editors: Thenkabail, P.S., Lyon, G.J., and Huete, A.). (Editors: Thenkabail, P.S., Lyon, G.J., and Huete, A.). IP-091722. Available at: https://www.routledge.com/Hyperspectral-Remote-Sensing-of-Vegetation-Second-Edition-FourVolume/Thenkabail-Lyon-Huete/p/book/9781138066250

Oksouei, M. and Babakan, S. 2016. Detection of Alteration Minerals Using Hyperion Data Analysis in Lahroud. *Journal of the Indian Society of Remote Sensing*, 44(5), 713-721.

Padarian, J., Minasny, B., McBratney, A., 2015. Using Google's cloud-based platform for digital soil mapping. *Computers and Geosciences*, 83, 80–88.

Padghan, M., and Deshmukh, R. 2017. Spectroscopic determination of aboveground biomass in grass using partial least square regression model. *International Journal of Scientific Engineering and Technology*, 6 (9), 332-335.

Panda, S. S., Rao, M.N., Thenkabail, P.S., Fitzerald, J.E. 2015. Remote Sensing Systems – Platforms and Sensors: Aerial, Satellites, UAVs, Optical, Radar, and LiDAR, Chapter 1. In Thenkabail, P.S., (Editor-in-Chief), 2015. "Remote Sensing Handbook" (Volume I): Remotely sensed data characterization, classification, and accuracies. ISBN 9781482217865 - CAT# K22125. Taylor and Francis Inc.\CRC Press, Boca Raton, London, New York. Pp. 3-60. IP-060641.

Pervez, W., Uddin, V., Khan, S., and Khan, J. 2016. Satellite-based land use mapping: Comparative analysis of Landsat-8, Advanced Land Imager, and big data Hyperion imagery. *Journal of Applied Remote Sensing*, 10, 026004-1–026004-20.

Ratheesh, R., Chaudhury, N., Rajput, P., Arora, M., Gujrati, A., Arunkumar, S., Shetty, A., Baral, R., Patel, R., Joshi, D., Patel, H., Pathak, B., Jayappa, K., Samal, R., and Rajawat, A. 2019. Coastal sediment dynamics, ecology and detection of coral reef macroalgae from AVIRIS-NG. *Current Science*, 116 (7), 1157-1165.

Rhee, D., Kim, Y., Kang, B., and Kim. D. 2018. Applications of unmanned aerial vehicles in fluvial remote sensing: An overview of recent achievements. *KSCE Journal of Civil Engineering*, 22 (2), 588-602.

Riaza, A., Buzzi, J., Garcia-Melendez, E., Carrere, V., Sarmiento, A., and Muller, A. 2014. Monitoring acidic water in a polluted river with hyperspectral remote sensing (Hymap). *Hydrological Sciences Journal*, DOI: 10.1080/02626667.2014.899704

Sacks, W., Deryng, D., Foley, J., Ramankutty, N., 2010. Crop planting dates: an analysis of global patterns. Global Ecology and Biogeography 19: 607-620. DOI: 10.1111/j.1466-8238.2010.00551.x.

SAGE. 2019. Crop Calendar Dataset. Available at: https://nelson.wisc.edu/sage/data-and-models/crop-calendar-dataset/index.php

Salem, S. 2017. ASD field hyperspectral measurements for discrimination of the ferruginous rocks and the iron ore types at El Gedida-Ghorabi area, Bahariya Oasis, Western Desert, Egypt. *Arabian Journal of Geosciences*, 10, 166.

Scheffler, D., Karrasch, P., 2014. Destriping of hyperspectral image data: An evaluation of different algorithms using EO-1 Hyperion data. *Journal of Applied Remote Sensing*, 8, 083645–1 to 083645–18.

Seidel, F., Kokhanovsky, A., Schaepman, M., 2010. Fast and simple model for atmospheric radiative transfer. *Atmospheric Measurement Techniques*, 3, 1129–1141.

Teluguntla, P., Thenkabail, P.S., Oliphant, A., Xiong, J., Gumma, M., Congalton, R., Yadav, K., and Huete, A. 2018. A 30-m Landsat-derived cropland extent product of Australia and China using random forest machine learning algorithm on Google Earth Engine cloud computing platform. *ISPRS Journal of Photogrammetry and Remote Sensing*, 144, 325-340.

Thenkabail, P.S., Lyon, G.J., and Huete, A. (Editors) 2018a. Book Title: Hyperspectral Remote Sensing of Vegetation (Second Edition, Four Volume-set). Volume I Title: Fundamentals, Sensor Systems, Spectral Libraries, and Data Mining for Vegetation. Publisher: CRC Press- Taylor and Francis group, Boca Raton, London, New York. Pp. 449, Hardback ID: 9781138058545; eBook ID:9781315164151.
https://www.routledge.com/Fundamentals-Sensor-Systems-Spectral-Libraries-and-Data-Mining-for-Vegetation/Thenkabail-Lyon-Huete/p/book/9781138058545

Thenkabail, P.S., Lyon, G.J., and Huete, A. (Editors) 2018b. Book Title: Hyperspectral Remote Sensing of Vegetation (Second Edition, Four Volume-set). Volume II Title: Hyperspectral Indices and Image Classifications for Agriculture and Vegetation. Publisher: CRC Press- Taylor and Francis group, Boca Raton, London, New York. Pp. 296. Hardback ID: 9781138066038; eBook-ID:9781315159331.
https://www.routledge.com/Hyperspectral-Indices-and-Image-Classifications-for-Agriculture-and-Vegetation/Thenkabail-Lyon-Huete/p/book/9781138066038

Thenkabail, P.S., Lyon, G.J., and Huete, A. (Editors) 2018c. Book Title: Hyperspectral Remote Sensing of Vegetation (Second, Edition, Four-volume-set). Volume III Title: Biophysical and Biochemical Characterization and Plant Species Studies. Publisher: CRC Press- Taylor and Francis group, Boca Raton, London, New York. Pp. 348. Hardback: 9781138364714; eBook ID: 9780429431180
https://www.routledge.com/Biophysical-and-Biochemical-Characterization-and-Plant-Species-Studies/Thenkabail-Lyon-Huete/p/book/9781138364714

Thenkabail, P.S., Lyon, G.J., and Huete, A. (Editors) 2018d. Book Title: Hyperspectral Remote Sensing of Vegetation (Second Edition, Four Volume-Set). Volume IV Title: Advanced Applications in Remote Sensing of Agricultural Crops and Natural Vegetation. Publisher: CRC Press- Taylor and Francis group, Boca Raton, London, New York. Pp. 386. Hardback: 9781138364769;-eBook-ID:9780429431166 https://www.routledge.com/Advanced-Applications-in-Remote-Sensing-of-Agricultural-Crops-and-Natural/Thenkabail-Lyon-Huete/p/book/9781138364769

Thenkabail, P., Mariotto, I., Gumma, M., Middleton, E., Landis, D., and Huemmrich, K. 2013. Selection of hyperspectral narrowbands (HNBs) and composition of hyperspectral two band vegetation indices (HVIs) for biophysical characterization and discrimination of crop types using field reflectance and Hyperion/ EO-1 data. *IEEE Journal of Selected Topics in Applied Earth Observations and Remote Sensing*, 6, 427–439.

Thenkabail, P.S. and Wu, Z. 2012. An Automated Cropland Classification Algorithm (ACCA) for Tajikistan by Combining Landsat, MODIS, and Secondary Data. *Remote Sensing*, 4, 2890-2918.

Thenkabail, P.S., Hanjra, M., Dheeravath, V. and Gumma, M. 2010. A Holistic View of Global Croplands and Their Water Use for Ensuring Global Food Security in the 21st Century through Advanced Remote Sensing and Non-remote Sensing Approaches. *Remote Sensing*, 2, 211-261.

Thenkabail, P., Enclona, E., Ashton, M., Legg, C., and de Dieu, M. 2014. Hyperion, IKONOS, ALI, and ETM+ sensors in the study of African rainforests. *Remote Sensing of Environment*, 90, 23–43.

Thompson, D., Seidel, F., Gao, B., Gierach, M., Green, R., Kudela, R., and Mouroulis, P. 2015. Optimizing irradiance estimates for coastal and inland water imaging spectroscopy. *Geophysical Research Letters*, 42, doi:10.1002/2015GL063287.

USDA, 2018a. CropScape- Cropland Data Layer. URL https://nassgeodata.gmu.edu/CropScape/

USDA, 2018b. CropScape and Cropland Data Layer- Metadata. URL https://www.nass.usda.gov/Research_and_Science/Cropland/metadata/meta.php

Verrelst, J., Romijn, E., and Kooistra, L. 2012. Mapping Vegetation Density in a Heterogeneous River Floodplain Ecosystem Using Pointable CHRIS/PROBA Data. *Remote Sensing*, 4, 2866-2889.

Xu, Q., Liu, S., Ye, F., Zhang, Z., and Zhang, C. 2018. Application of CASI/SASI and fieldspec4 hyperspectral data in exploration of the Baiyanghe uranium deposit, Hebukesaier, Xinjiang, NW China. *International Journal of Remote Sensing*, 39 (2), 453-469.

Zhang, J., Rivard, B., Sanchez-Azofeifa, A., and Castro-Esau, K. 2006. Intra- and inter-class spectral variability of tropical tree species at La Selva, Costa Rica: Implications for species identification using HYDICE imagery. *Remote Sensing of Environment*, 105, 129-141.